Journal of Materials Chemistry C

ROYAL SOCIETY OF CHEMISTRY

PAPER

View Article Online
View Journal

Cite this: DOI: 10.1039/d5tc02038g

1,2,5,6-Tetrathiocin as a scaffold for improved charge transport in double-cable oligothiophene systems

Rupert G. D. Taylor, [a] Joseph Cameron, [b] Michael Fairley,[a] Iain A. Wright, [c] Lisa R. Savagian, [a] Claire Wilson, [bd] Mateusz B. Pitak, [d] Simon J. Coles, [d] Manikanta Makala, [e] Oana D. Jurchescu *[e] and Peter J. Skabara *[b]

Received 23rd May 2025,
Accepted 16th August 2025

DOI: 10.1039/d5tc02038g

rsc.li/materials-c

Four novel small molecules featuring central 1,2,5,6-tetrathiocin (TTC) units fusing two oligothiophene chains have been prepared, characterised and their structures elucidated through X-ray crystallography. These compounds have been evaluated as p-channel semiconductors in organic field-effect transistor devices, representing the first time that any tetrathiocin-containing compound has been utilised in organic transistors. Through extensive optimisation, involving the screening of different processing solvents, surface treatments, post-processing conditions, dielectric materials, and device configurations, hole mobilities (μ_h) in the 10^{-2} cm^2 V^{-1} s^{-1} range were obtained for the most optimised devices, with the highest value of 7.3×10^{-2} cm^2 V^{-1} s^{-1} achieved in **5T-TTC**. The double-cable design, established through two parallel oligothiophene chains in the same molecule bridged by a tetrathiocin core, provides improved device characteristics over analogous double-cable oligothiophenes with tetrathiafulvalene and germanium cores.

Introduction

Interest in organic materials as semiconductors in field-effect transistors is strong due to their ability to match or better the mobility (μ) of amorphous silicon,[1–5] whilst offering a number of processing advantages.[6] These include: the capacity for deposition from solution, removing the high costs associated with vacuum deposition at high temperature and/or low pressure, flexibility, allowing for the use of light-weight flexible substrates, and chemical tunability, allowing for functional molecular design of the required structure–property relationship. Polymeric organic materials are used in organic field-effect transistors (OFETs) and other organic electronic devices (*e.g.* organic photovoltaics),[7] as their long polymer chains can result in excellent film quality when processed from solution. However, due to the nature of polymerisation reactions, the resultant polymers often show significant variation in molecular weight, polydispersity and end-group functionality, resulting in batch-to-batch variation of the polymers and subsequent devices. In comparison, well-defined and solution-processable oligomeric functional organic components provide some important advantages as their batch-to-batch reproduction is higher and they are easier to purify due to their monodisperse nature.[8–10]

Dimensionality plays a critical role in charge transport in organic semiconductors.[11,12] Whilst the overlap of frontier molecular orbitals is more significant in one-dimensional materials, for example between disc-like molecules, charge transport relies on molecular orbital overlap in the bulk and is therefore more efficient in higher-dimensionality structures.[11] Ideally, therefore, an organic semiconductor will have good orbital overlap between molecules in the bulk in two dimensions, whilst finding a true 3D organic semiconductor is rare.[13] In the quest for higher dimensionality, oligomers possessing two chains of conjugated units are exciting candidates, especially if they can supply a greater number of non-covalent contacts, for example through heteroatom–heteroatom or π–π interactions. Indeed, short-range non-covalent interactions have been reported to influence solid-state organisation in conjugated polymers, resulting in enhanced charge transport.[14] Previously, we have reported two series of molecules featuring 'double-cable' oligothiophene chains, with terthiophene (3T), quinquithiophene (5T) and septithiophene (7T)

[a] *WestCHEM, Department of Pure and Applied Chemistry, University of Strathclyde, Glasgow, G1 1XL, UK*
[b] *School of Chemistry, University of Glasgow, Glasgow, G12 8QQ, UK. E-mail: peter.skabara@glasgow.ac.uk*
[c] *School of Chemistry, University of Edinburgh, Edinburgh, EH9 3FJ, UK*
[d] *School of Chemistry, University of Southampton, Southampton SO17 1BJ, UK*
[e] *Department of Physics and Center for Functional Materials, Wake Forest University, Winston-Salem, NC 27109, USA. E-mail: jurchescu@wfu.edu*

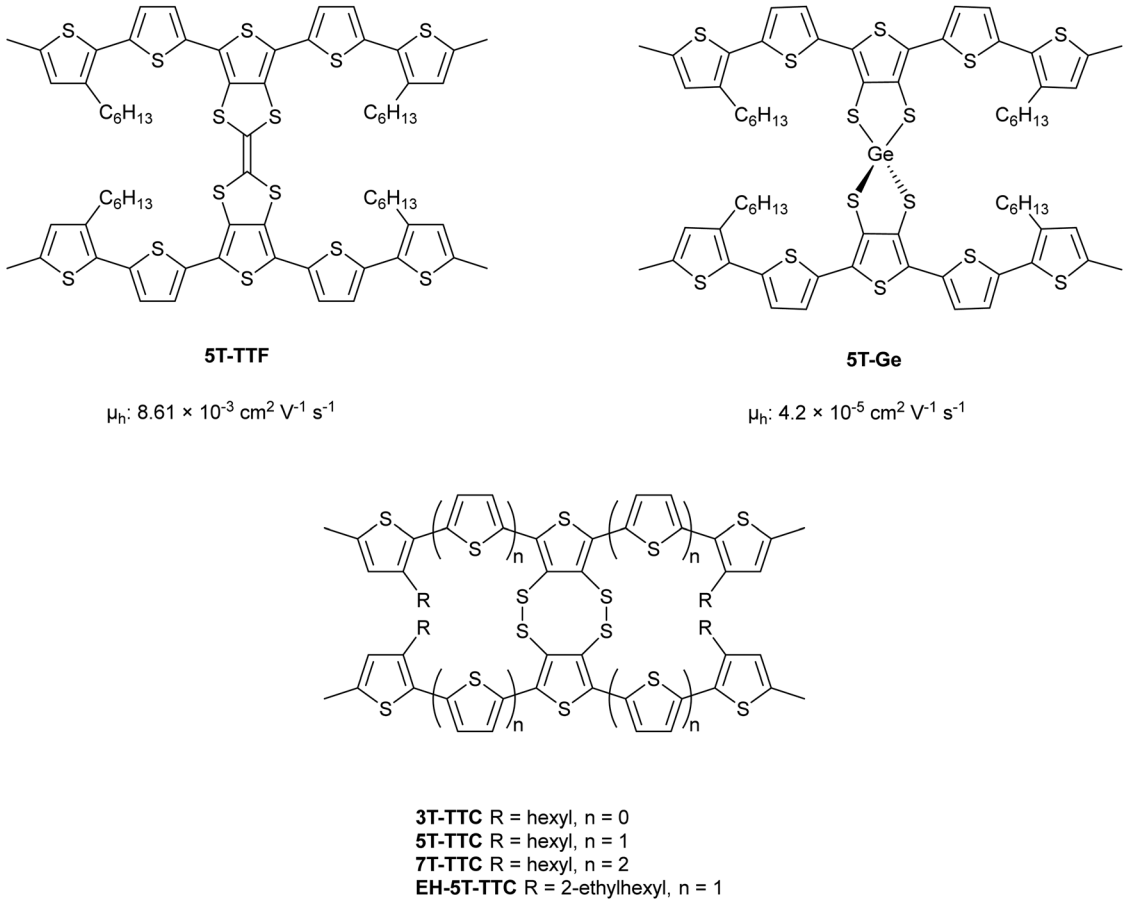

Fig. 1 Molecules with 'double-cable' oligiothiophene chains: **5T-TTF** (top left),[15] **5T-Ge** (top right),[18,19] and **oligothiophene TTCs** (bottom, centre. This work).

units fused to either a tetrathiafulvalene (TTF)[15–17] or a germanium atom spirocentre core[18,19] (the quinquithiophenes **5T-TTF** and **5T-Ge** are shown as examples in Fig. 1). In all cases, the oligothiophenes feature hexyl chains for solubility and terminal methyl groups for redox stability (*i.e.* to eliminate the possibility of the oligomers polymerising upon oxidation). In other previous work, we reported a new 5T analogue with a tetrathiocin core (**EH-5T-TTC**, Fig. 1), and its function as a ternary material in organic solar cells.[20] Here, we evaluate the charge transport properties of this material in OFETs, and also introduce and assess the OFET performance of three new tetrathiocin analogues.

Compounds featuring the 1,2,5,6-tetrathiocin moiety have previously been studied owing to their interesting twist or chair-like conformations (Fig. 2). Calculations have shown that for the parent 1,2,5,6-tetrathiocin molecule, the twist conformation is of the lowest energy, and that the chair conformation is readily accessible (5.3 kcal mol^{-1}).[21–23] Tetrathiocins have shown use as precursors to benzodithiins[24] and dithiolate ligands in group 10 metal complexes,[25–27] and for their biological activity,[28–30] but they have never been studied as a components of molecules or polymers used in organic electronics.

Fig. 2 1,2,5,6-Tetrathiocin in the twist (left) and chair (right) conformations.

Synthesis

The oligothiophene-functionalised 1,3-dithiole-2-one compounds **5a–d** were prepared in accordance with the published procedures.[15,16,20] The general route (Scheme 1),[31] involved the reaction of lithiated vinylene trithiocarbonate (**1**) with the corresponding formyl oligothiophene (**2a–d**), followed by oxidation to give the dicarbonyl derivatives **3a–d**. The 1,3-dithiole-2-thione compounds were then transchalcogenated using $Hg(OAc)_2$ to give the carbonyl derivatives **4a–d**, which subsequently underwent Paal–Knorr cyclisation with phosphorus pentasulfide to give the oligothiophenes **5a–d**. Tetrathiocins **3T-TTC**, **5T-TTC**, **7T-TTC** and **EH-5T-TTC** were prepared in one pot from their respective half-units (**5a–d**), by first reacting the 1,3-dithiol-2-one unit with freshly prepared sodium methoxide, generating a dithiolate *in situ* which was then oxidised with iodine forming the disulfide bonds. **EH-5T-TTC** exhibits

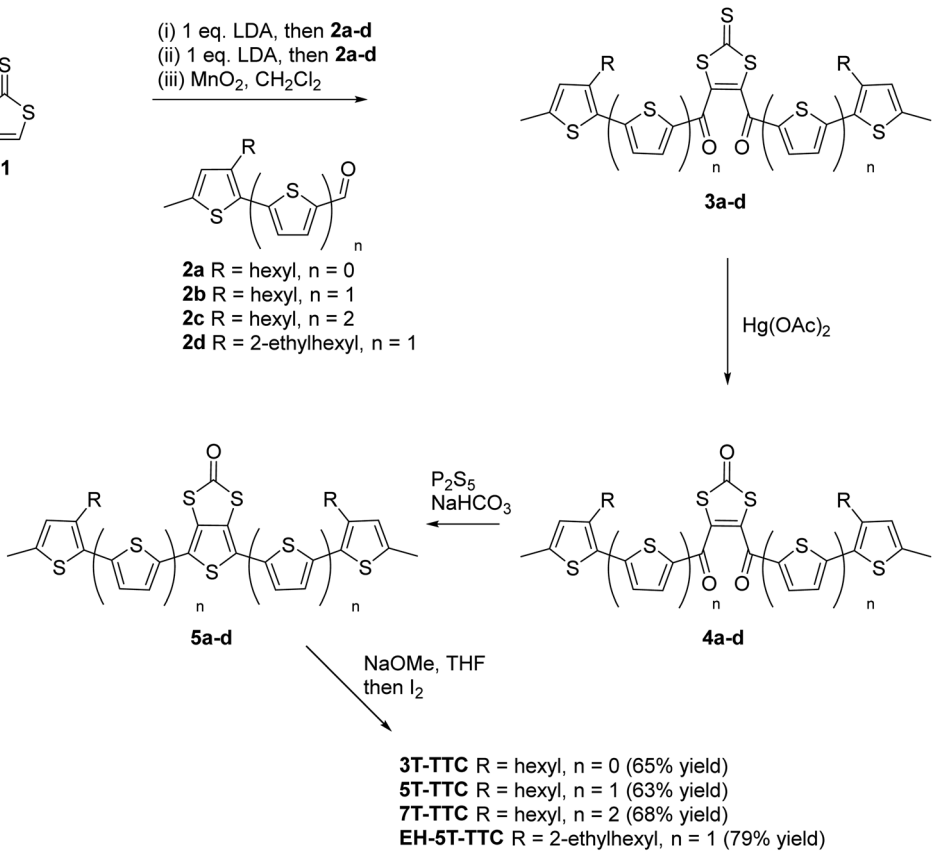

Scheme 1 Synthesis of the tetrathiocin derivatives **3T-TTC**, **5T-TTC**, **7T-TTC** and **EH-5T-TTC**.

significantly improved solubility over **5T-TTC**. The solubility of **5T-TTC** in dichloromethane is 1–2 mg ml^{-1} at room temperature, whilst at the same temperature **EH-5T-TTC** has a solubility > 30 mg ml^{-1}.

Crystallography

Crystals of **5b**, **3T-TTC** and **5T-TTC** were obtained and analysed by single-crystal X-ray diffraction studies. The structure of compound **EH-5T-TTC** was previously reported.[20] Of particular interest in these structures are the following questions, which are important in understanding the impact of molecular design on promoting efficient orbital overlap in the bulk material: (i) is there an optimum length of the oligothiophene in supporting planarity in the conjugated chain? (ii) does the choice of alkyl chain (linear *vs.* branched) make a difference to the solid-state packing? (iii) is there any benefit in the double-cable design of the molecules and, if so, does the unusual tetrathiocin unit have an important role to play?

The molecular structures of **5b**, **3T-TTC** and **5T-TTC** are shown in Fig. 1. For the tetrathiocin structures (**3T-TTC** and **5T-TTC**), the central 8-membered ring adopts a chair conformation, rather than a twist. There is an inversion symmetry with the centre positioned in the tetrathiocin ring. In the case of **5T-TTC** there are two independent molecules in the asymmetric unit with slight differences only in bond lengths and angles. In both of the quinquithiophene (5T) structures, the thiophenes are arranged in an *anti* conformation apart from one of the terminal thiophenes in each chain, which adopts a *syn* arrangement. In the case of **5T-TTC**, this could be explained by the unfavourable steric effect that an all-*anti* conformation would have, *viz.* the direct overlap of the hexyl chains between the 5T chains in the single molecule tetrathiocin structure. However, the conformation of the half-unit **5b** is not restricted in such a manner, yet still retains the *syn* arrangement for one of the peripheral thiophene rings. The torsion angles between the thiophene rings for each of the compounds are shown in Fig. 3 and these have been measured through the corresponding S–C–C–S units. In the 5T compounds, the thiophene rings with *anti* conformations are highly co-planar, but the torsion angles for the *syn* conformers range from 30.58° to 37.95°, indicating a reasonable loss of conjugation in those units. In the terthiophene, the three thiophene rings in each chain are highly twisted from each other, with torsion angles of 57.13° and 67.61°. This is surprising, since an all-*anti* conformer would have the four hexyl groups pointing away from each other, eliminating any conformational bias due to steric reasons.

The packing motifs of compounds **3T-TTC** and **5T-TTC** are represented in Fig. 4. In the first diagram (Fig. 4a), stacks of the quinquithiophene-tetrathiocin molecules are shown, in which the double-cable oligothiophene chains overlap in one dimension. Between these stacks, the hexyl groups insulate the

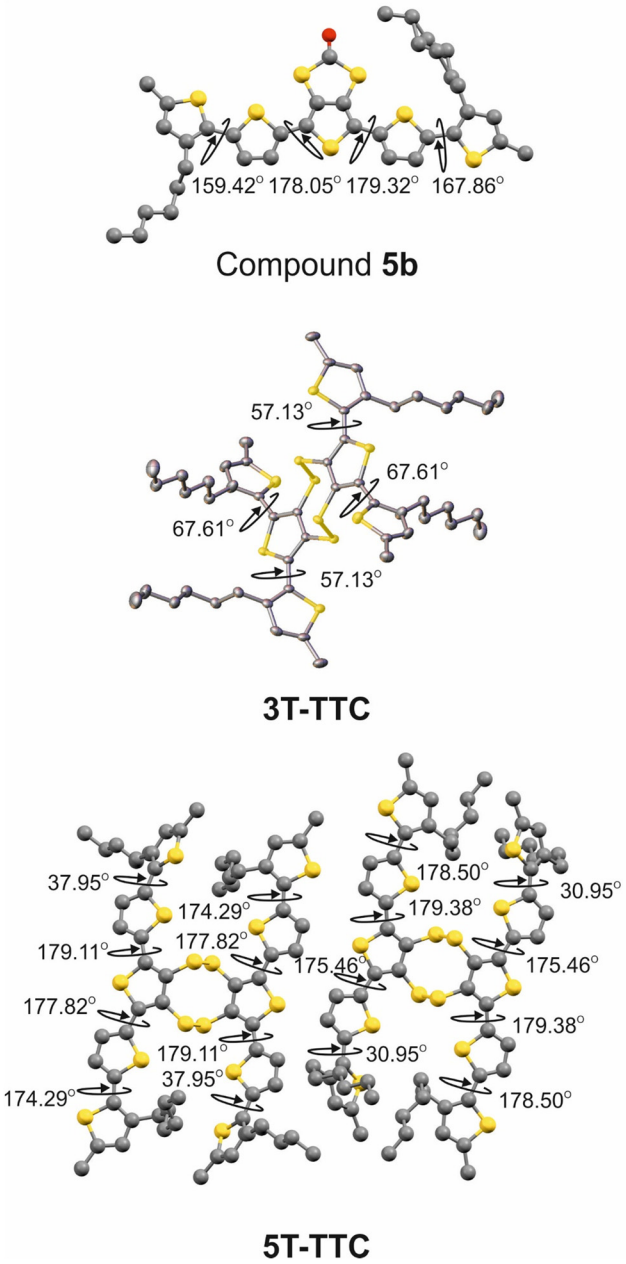

Fig. 3 Structures of the compounds **5b**, **3T-TTC** and **5T-TTC** determined by single-crystal X-ray diffraction studies.

conjugated units and prevent orbital overlap in this dimension (left to right in Fig. 4a). Fig. 4b shows the arrangement of the molecules of **5T-TTC** within a stack and identifies two sets of S···S short contacts – interactions between the sulfur atoms in overlapping tetrathiocin rings (3.508 Å, shown in red), and S···S interactions between one tetrathiocin sulfur atom and that of an overlapping thiophene ring (3.501 Å, shown in blue). These short contacts are less than the sum of the van der Waals radii for two sulfur atoms (3.6 Å). In addition to these chalcogen-based interactions, the oligothiophene chains between overlapping molecules feature π–π interactions through each of the double-cable conjugated 5T units (3.598 Å, Fig. 4c).

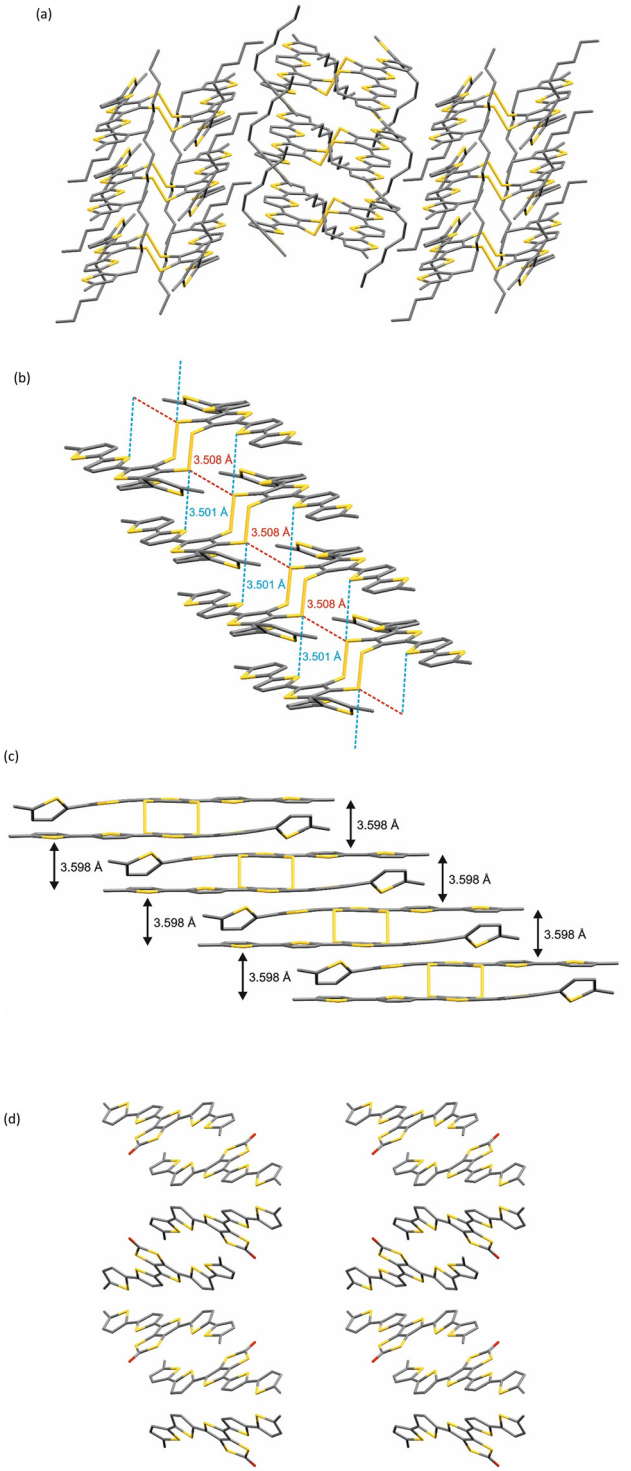

Fig. 4 Packing diagrams for compounds **5b** and **5T-TTC** showing (a) arrangements of stacks in **5T-TTC**, (b) close S···S contacts between the tetrathiocin molecules in **5T-TTC**, (c) π–π stacking distances between chains of quinquithiophenes in **5T-TTC**, and (d) arrangement of **5b** molecules viewed along the *c* axis. In figures (b)–(d), the hexyl groups have been omitted for clarity.

Furthermore, the oligothiophene chains overlap in a staggered, step-wise fashion, meaning that the combination of chalcogen

interactions and π-interactions give orbital overlap in two dimensions. There are no heteroatom contacts or π–π interactions observed in the structure of **5b** with the molecules effectively isolated from each other (Fig. 4d). This illustrates the benefit of incorporating the tetrathiocin structure in the 5T system, which fosters S···S contacts and the formation of π–π stacks. Concerning the conformation of the tetrathiocin unit, the chair structure supports close contact between chains, whereas a twisted conformation in this ring would not be a rigid one (as seen, for example, in the Ge-centred analogue 5T-Ge), and would not favour π–π stacking. We can therefore conclude from the X-ray diffraction studies that at least a quinquithiophene 5T chain is necessary for effective conjugation, and that the integration of a tetrathiocin ring to give a double-cable structure is indeed beneficial for high dimensionality in the bulk through non-covalent interactions.

Thermal properties

The thermal properties of the materials were studied using thermogravimetric analysis (TGA) and differential scanning calorimetry (DSC). The TGA plots of are shown in Fig. S7–S10, the DSC plots in Fig. S11–S14 and the results are summarised in Table 1. The temperature at 5% mass loss ($T_{95\%}$) increases as the conjugation length across the series increases, as expected. **EH-5T-TTC** has a lower $T_{95\%}$ than **5T-TTC**, which suggests an instability caused by the presence of the ethylhexyl chain. A similar observation has been noted by Zhang and co-workers in alkylthiothiophene-substituted benzo[1,2-*b*:4,5-*b*′]dithiophene-based polymers with octyl and 2-ethylhexyl side groups.[32] However, with all degradation temperatures close to or above 300 °C, the materials can be deemed thermally stable for operation in organic semiconductor devices.

In analysing the DSC data, it can be observed that the melting point increases with increasing conjugation length. **5T-TTC** and **7T-TTC** exhibit interesting behaviour (Fig. S12 and S14, respectively), where two sharp melting points can be observed in the heating cycles of these compounds. This suggests the presence of two different crystalline phases in these molecules. Only in the DSC plot of **7T-TTC** is there a crystallisation peak observed in the temperature range, while no glass transitions can be noticed.

Optical properties

Absorption spectra of the tetrathiocin compounds (Fig. 5), reveal the expected red-shifting of peak maxima as the conjugation length increases, with solution-state maxima of 318, 431 and 461 nm for the longest wavelength peaks (π–π* transitions) of **3T-TTC**, **5T-TTC** and **7T-TTC**, respectively. **EH-5T-TTC** gives very similar spectra to **5T-TTC** both in solution and solid-state, showing that the added bulk due to the branched nature of the alkyl chain does not disrupt the conjugation of the oligothiophene system. The apparent red-shifting of the solid-state onset for **5T-TTC** *vs.* **EH-5T-TTC** is likely due to scattering caused by the poor film quality as a result of the poor solubility of **5T-TTC**. The smaller red shift between **5T-TTC** and **7T-TTC** (*vs.* **3T-TTC** to **5T-TTC**) is due to the effective conjugation length not spanning the entire septithiophene chains of **7T-TTC**.[33] When compared to the UV spectra of their half-units (**5a–d**), each of the tetrathiocins shows a slightly blue-shifted peak maximum, confirming that there is no conjugation between the two oligothiophene chains across the tetrathiocin core. Using the onset of the longest wavelength solution-state absorption peaks, optical HOMO–LUMO (highest occupied molecular orbital, lowest unoccupied molecular orbital) gaps are calculated as 3.06, 2.40, 2.41 and 2.25 eV for **3T-TTC**, **5T-TTC**, **EH-5T-TTC** and **7T-TTC**, respectively.

Due to the lower solubility and high crystallinity of **5T-TTC** and **7T-TTC**, their solid-state absorption spectra exhibit significant scattering at high wavelengths due to poor film quality (Fig. 5, right). As such, determination of solid-state optical HOMO–LUMO gaps are rough estimates, though the relevant data is given in Table 1.

Table 1 Summary of thermal properties determined using TGA and DSC

	$T_{95\%}$ (°C)	T_m (°C)	T_c (°C)
3T-TTC	297.9	128.6	Not observed
5T-TTC	348.1	212.1, 214.5	Not observed
EH-5T-TTC	318.4	143.3	Not observed
7T-TTC	365.4	163.5, 220.5	146.1

Electrochemical properties

In order to establish their electrochemical properties, cyclic voltammetry (CV) was performed on dichloromethane solutions (10^{-4} M) of the four tetrathiocin compounds. The oxidation plots of **3T-TTC**, **5T-TTC** and **EH-5T-TTC** (Fig. 6) reveal well-defined, reversible (or quasi-reversible) oxidations that allow for calculation of the respective HOMO energy levels (Table 2). However, the oxidation of **7T-TTC** is far more complex, resulting in a broad non-discrete peak caused by multiple oxidation processes occurring within a narrow potential window. Such a result has been previously reported where the identical septithiophene chains were fused to a tetrathiafulvalene core.[16] As a result, no estimation of the HOMO level of **7T-TTC** is given.

3T-TTC shows a first reversible oxidation at a peak potential of +0.78 V, followed by an irreversible oxidation at +1.08 V. The latter appears to be a two-electron process, though is more likely to be two overlapping one-electron oxidations. As expected, **5T-TTC** and **EH-5T-TTC** show essentially identical plots with initial reversible oxidations occurring at peak potentials of +0.46/+0.48 V, followed by a second reversible oxidation at *ca.* +0.60/+0.61 V, and an irreversible oxidation at +0.69/+0.72 V. These oxidation potentials result in HOMO levels of −5.26 and −5.28 eV for **5T-TTC** and **EH-5T-TTC**, respectively, whilst **3T-TTC** shows a deeper HOMO level at −5.58 eV (values estimated from the HOMO energy level of ferrocene, used as a reference and taken as −4.8 V).

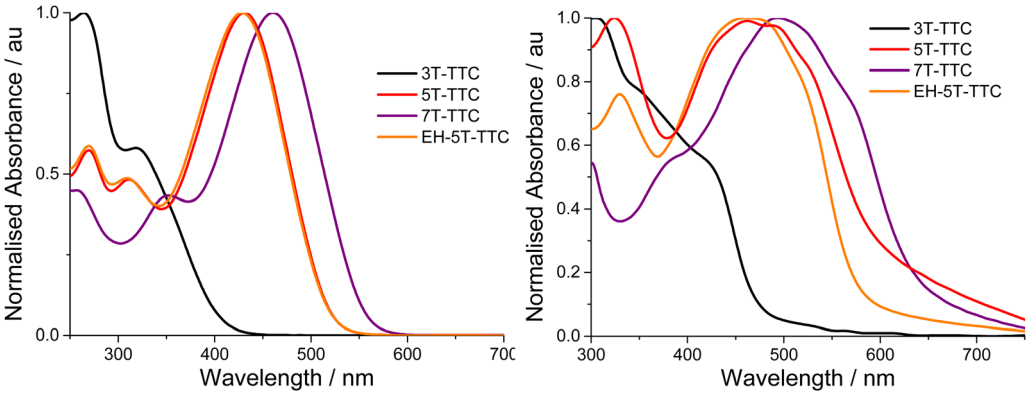

Fig. 5 Absorption spectra of the four tetrathiocin molecules in dichloromethane solution at 10^{-5} M (left), and as thin films cast from chlorobenzene solution (right).

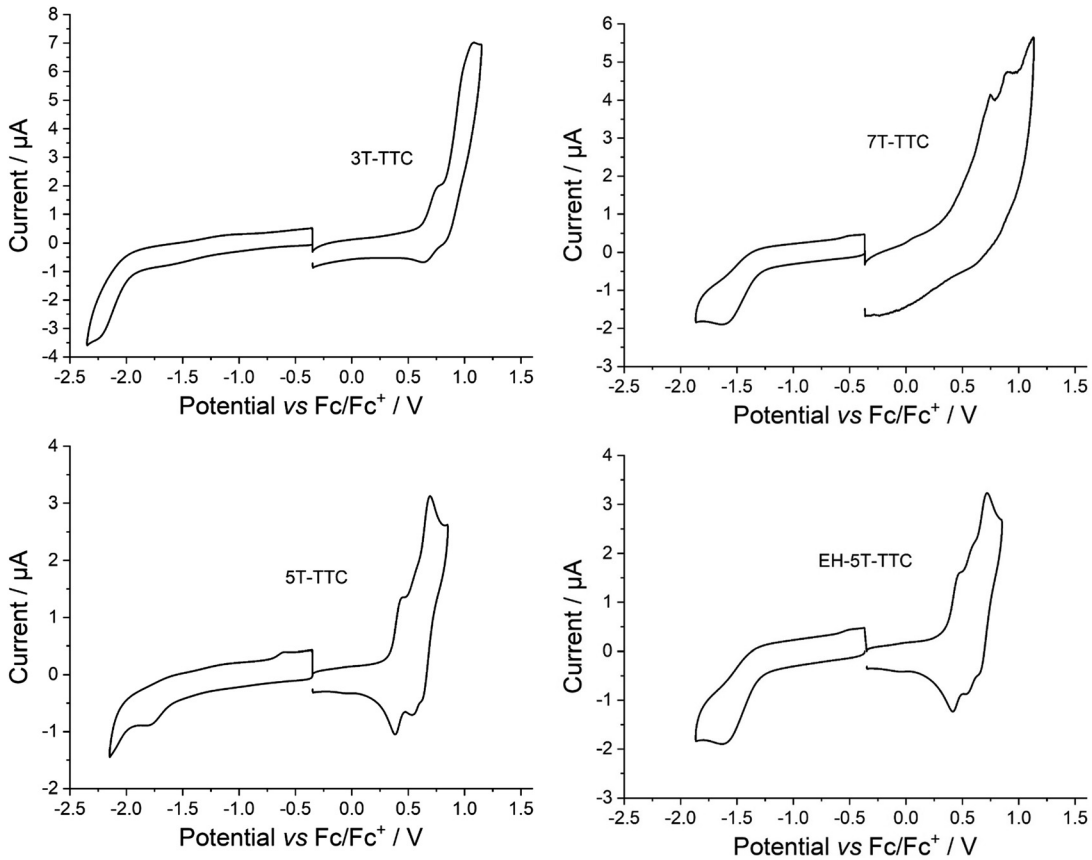

Fig. 6 Reduction and oxidation voltammograms, recorded separately. Measured in dichloromethane solution at 10^{-4} M using 0.1 M $^{n}Bu_4NPF_6$ as the supporting electrolyte (100 mV s^{-1} scan rate). Glassy carbon disc, silver wire and platinum wire were used as the working, quasi-reference and counter electrodes, respectively. The data are referenced to the ferrocene/ferrocenium redox couple (E_{HOMO} = −4.8 eV).

At negative potentials, irreversible reductions are revealed at peak potentials of −2.25, −1.81, −1.86 and −1.61 V for **3T-TTC**, **5T-TTC**, **EH-5T-TTC** and **7T-TTC**, respectively. Consequently, **5T-TTC** and **EH-5T-TTC** are found to possess essentially the same electrochemical HOMO–LUMO gap (2.27 and 2.34 eV, respectively), whilst **3T-TTC** has a much wider gap at 3.33 eV. Accurate determination of the electrochemical HOMO–LUMO gap for **7T-TTC** is not possible owing to the broad non-discrete nature of the oxidation. However, taking the most apparent onset of oxidation to be at +0.34 V leads to an estimated HOMO level of 5.14 eV and an electrochemically determined HOMO–LUMO gap of 1.95 eV.

Table 2 Optical, electrochemical and thermal properties of the TTC molecules

	Solution		Solid state						
	λ_{max}[a] (nm)	λ_{onset}[a] (nm)	E_g opt.[b] (eV)	λ_{max} (nm)[c]	λ_{onset} (nm)[c]	HOMO[d] (eV)	LUMO[d] (eV)	E_g elec. (eV)	T_d (°C)
3T-TTC	264	406	3.05	309	468	−5.58	−2.55	3.33	298
5T-TTC	431	516	2.40	459	588	−5.26	−2.99	2.27	348
7T-TTC	461	552	2.25	494	632	—	−3.19	—	366
EH-5T-TTC	429	515	2.41	460	574	−5.28	−2.94	2.34	319

[a] Obtained from dichloromethane solutions at 10^{-5} M. [b] Calculated from the onset of the longest wavelength absorption peak. [c] Obtained from thin films cast from chlorobenzene. [d] Calculated from CV (dichloromethane solutions at 10^{-4} M), using the peak potential referenced to the ferrocene/ferrocenium redox couple (E_{HOMO} = −4.8 eV).

Charge transport and device performance in OFETs

The series of tetrathiocin-bearing oligothiophenes was tested in OFETs to characterise their charge transport properties. Since the compound **3T-TTC** did not feature any close contacts in its crystalline state, we did not study this material in OFETs. Two device geometries, top gate/bottom contact (TGBC) and bottom gate/bottom contact (BGBC), were used to analyse charge transport in these materials,[34] as shown in Fig. 7a and b. Prior to the deposition of organic semiconductor, the silicon oxide substrate and/or the gold contacts were treated with octadecyltrichlorosilane (OTS) and pentafluorobenzenethiol (PFBT) self-assembled monolayers, respectively. These treatments play a crucial role in modifying the surface properties of the electrodes – OTS creates a hydrophobic surface,[35] reducing trap generation[36,37] at the semiconductor/dielectric interface, while PFBT improves charge injection by tuning the electrode work function.[38–40] The TTC film was spin-coated from a solution in chlorobenzene or chloroform, followed by annealing at different temperatures (as-cast, 60 °C, 90 °C, or 120 °C). Further details on experimental procedures can be found in the SI. Note that the use of carbon disulfide as a cosolvent for **5T-TTC** and **7T-TTC** was required to reach concentrations (*ca.* 10 mg ml^{-1}) for suitable film quality. It should be noted that the bulk film morphology of **5T-TTC** and **7T-TTC** was poor due to the necessity to use carbon disulfide, which is highly volatile, for dissolution. The deposited films were sufficient for measurements on the length scales for OFET channels but over a larger area such films would be considered unsuitable for thin-film devices such as organic photovoltaics. The improved solubility due to the use of branched alkyl chains in **EH-5T-TTC** avoids the problem. The device characteristics for **5T-TTC** and **EH-5T-TTC** are collated and presented in Tables 3 and 4,

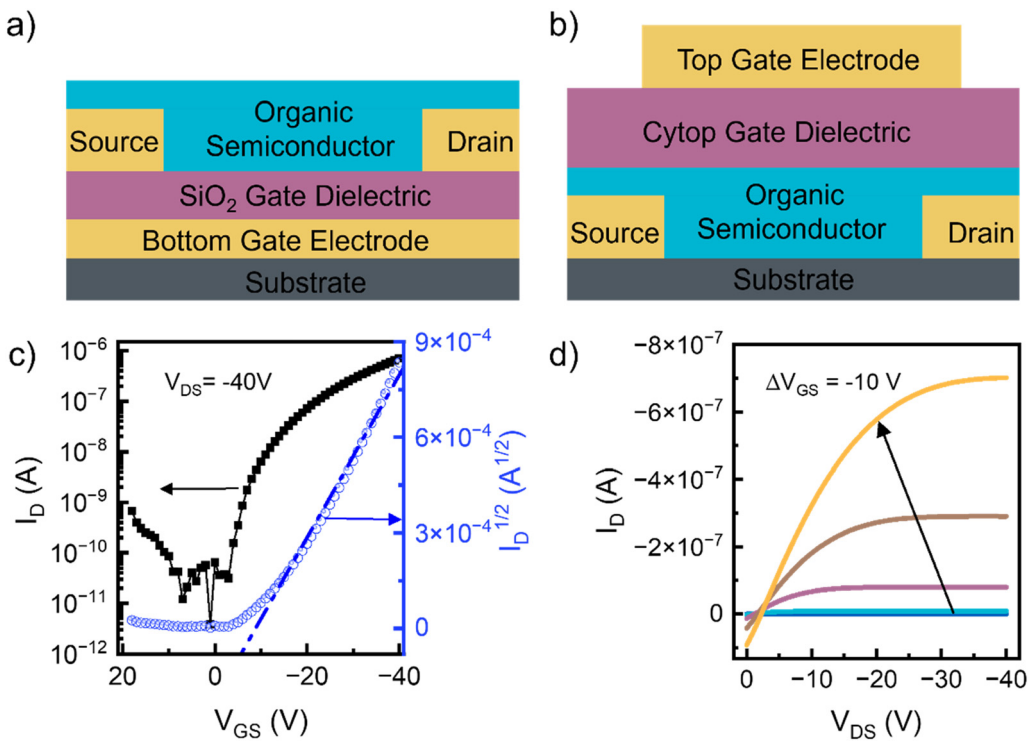

Fig. 7 Bottom-gate bottom-contact (a) and top-gate bottom-contact (b) OFET device structures, with representative transfer (c) and output (d) characteristics.

Table 3 OFET data for compounds **5T-TTC** from devices using SiO_2 and Cytop as the dielectric layers. Values reported are taken as average from a minimum of four devices

Gate dielectric	Solvent	SAM	Annealing temperature (°C)	μ_h ($cm^2\ V^{-1}\ s^{-1}$)	V_{th} (V)	I_{on}/I_{off}
SiO_2	Chloroform/CS_2 2 : 1	OTS/PFBT	As cast	1.8×10^{-2}	−33	10^5
			60	2.0×10^{-2}	−27	10^5
			90	7.0×10^{-3}	−17	10^4
			120	1.7×10^{-2}	−27	10^5
	Chlorobenzene/CS_2 2 : 1	OTS	As Cast	4.3×10^{-3}	−23	10^3
			60	5.3×10^{-3}	−21	10^3
			90	1.3×10^{-3}	−17	10^2
			120	7.1×10^{-4}	−16	10^2
	Chlorobenzene/CS_2 2 : 1	OTS/PFBT	As cast	8.1×10^{-4}	−22	10^2
			60	1.1×10^{-2}	−27	10^3
			90	2.0×10^{-3}	−18	10^3
			120	5.6×10^{-3}	−17	10^3
Cytop	Chlorobenzene/CS_2 2 : 1	PFBT	As cast	5.5×10^{-2}	−9	10^3
			60	5.0×10^{-2}	−6	10^2
			120	3.0×10^{-2}	−10	10^2

Table 4 OFET data for compounds **EH-5T-TTC** from devices using SiO_2 and Cytop as the dielectric layers. Values reported are taken as average from a minimum of four devices

Gate Dielectric	Solvent	SAM	Annealing temperature (°C)	μ_h ($cm^2\ V^{-1}\ s^{-1}$)	V_{th} (V)	I_{on}/I_{off}
SiO_2	Chloroform	OTS/PFBT	As cast	5.5×10^{-3}	−35	10^4
			60	2.1×10^{-2}	−31	10^4
			90	2.9×10^{-3}	−28	10^3
			120	3.6×10^{-4}	−19	10^3
	Chlorobenzene	OTS/PFBT	As cast	3.4×10^{-3}	−37	10^3
			60	5.0×10^{-3}	−27	10^3
			90	7.7×10^{-4}	−30	10^3
			120	2.4×10^{-4}	−23	10^2
Cytop	Chlorobenzene	PFBT	As cast	1.7×10^{-2}	−12	10^5
			60	3.0×10^{-2}	−13	10^4
			120	3.0×10^{-2}	−8	10^5

respectively, while representative transfer and output characteristics are reported in Fig. 7c and d; the characteristics of all devices are shown in Fig. S15–S35, S37–S39.

It was observed that the use of PFBT resulted in higher OFET performance which we assign to the reduction in the injection barrier and surface energy,[38,41] the first yielding lower contact resistance and the latter resulting in variance in morphologies of the films as a function of their different alkyl substituents. For both **5T-TTC** and **EH-5T-TTC**, the values of hole mobilities observed in bottom-gate, bottom contact OFETs was in the range 7.7×10^{-4} to 2.1×10^{-2} $cm^2\ V^{-1}\ s^{-1}$. The best performance for **5T-TTC** (2.0×10^{-2} $cm^2\ V^{-1}\ s^{-1}$, on/off ratio of 10^5) was achieved using $CHCl_3/CS_2$ as the solvent for spin-coating the semiconductor, whilst that of **EH-5T-TTC** (2.1×10^{-2} $cm^2\ V^{-1}\ s^{-1}$, on/off ratio of 10^4), was obtained from deposition from a chloroform solution. Both these sets of devices were annealed at 60 °C and used both OTS and PFBT surface treatments. In fact, the performance of OFETs annealed at 60 °C was always highest compared to those annealed at higher temperatures or not annealed, regardless of the fabrication conditions.

Atomic force microscopy (AFM) was used to gain further insight into the influence of processing conditions on OFET performance. The impact of annealing temperature was studied for devices containing **5T-TTC** processed from $CHCl_3/CS_2$ on PFBT/OTS-modified substrates. The topography images for the different films are shown in Fig. S36(a)–(d). While the general topography looks very similar for the different films, which is consistent with the small deviation in performance, there is a clear improvement in film quality for the film annealed at 60 °C (Fig. S36b). This film shows smaller domains with more uniform coverage compared to those not annealed or annealed at higher temperature, suggesting the balance between solvent evaporation rate and thermal energy for more favourable reorganisation of molecules is best achieved at 60 °C.

Whilst both **5T-TTC** and **EH-5T-TTC** gave similar device performance in BGBC geometry, there is a clear advantage in having the branched 2-ethylhexyl chain in **EH-5T-TTC** as the higher solubility means that carbon disulfide is not required for the solution-processing. The resulting films are also of better quality as observed from topography images shown in Fig. 8. The topography of **EH-TTC** shows a more uniform film with root-mean-square roughness (R_q) of 1.8 nm compared to 19.9 nm for the film **5T-TTC**. The film of **5T-TTC** shows larger domains that its analogue, due to its propensity to aggregate. While this is an advantage for molecular ordering, a key parameter for high charge mobility, the performance of **EH-5T-TTC** shows that the inclusion of branched alkyl chains can realise a compromise between processability and maintaining close intermolecular contacts.

The effect that the solvent choice has on the deposited films was also studied by examining AFM topography images. In **EH-5T-TTC**, where films have been annealed at 60 °C, there is a large performance difference in hole mobility dependent on the solvent used for deposition (2.1×10^{-2} $cm^2\ V^{-1}\ s^{-1}$ *vs.* 5.0×10^{-3} $cm^2\ V^{-1}\ s^{-1}$ when chloroform or chlorobenzene

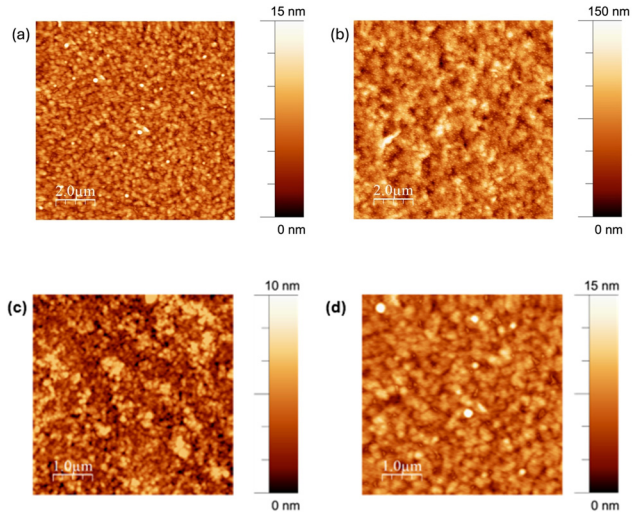

Fig. 8 Atomic force microscopy topography images (10 × 10 μm^2 scan area) of films of (a) **EH-5T-TTC** and (b) **5T-TTC** in the bottom gate, bottom contact OFETs which exhibited the highest hole mobility. Both materials were deposited onto PFBT and OTS modified substrates and annealed at 60 °C. **EH-5T-TTC** was deposited from $CHCl_3$, while **5T-TTC** was deposited from $CHCl_3/CS_2$ (2 : 1). Atomic force microscopy topography images (5 × 5 μm^2 scan area) of **EH-5T-TTC** films deposited from (c) chlorobenzene (R_q = 1.5 nm) and (d) chloroform (R_q = 1.8 nm) in bottom-gate, bottom-contact OFETs modified using PFBT and OTS, annealed at 60 °C.

are used, respectively). Fig. 8(c) and (d) shows the topography images of these films and there is a similar low roughness, with R_q values of 1.5 nm and 1.8 nm when **EH-5T-TTC** is deposited from chlorobenzene or chloroform, respectively. However, the film formed by depositing using a chlorobenzene shows more 'islands' and a lack of connectivity between domains which can be expected to be detrimental to the charge mobility.

We followed the same experimental procedures for characterising **7T-TTC**, and observed that in this case only devices which were not subject to thermal annealing functioned as OFETs, with modest transistor characteristics: average mobility of 2.8×10^{-5} cm^2 V^{-1} s^{-1}, threshold voltage of −17 V and on/off ratio of ∼80. These devices contained PFBT and OTS SAMs and the solutions were deposited from $CHCl_3/CS_2$ solution, but films formed were of poor quality. These results suggest that increased conjugation length of this molecule increases the formation of aggregates, resulting in rougher films forming upon spin-coating. The observations from **7T-TTC**-based devices are consistent with our previous report on the hole mobility of an analogous system, **7T-TTF**, determined to be $\sim 1.5 \times 10^{-5}$ cm^2 V^{-1} s^{-1}.[16] However, with side chain engineering to improve solubility and favourable aggregation, it is possible that **7T-TTC** systems could be improved, given α-septithiophene has previously been reported to have slightly higher hole mobilities than α-quinquithiophene.[42]

The initial experimental results on the quinquithiophene derivatives encouraged us to further optimise the performance of **5T-TTC** and **EH-5T-TTC** OFETs using Cytop top-gate dielectric, which has the device geometry shown in Fig. 7b. Despite the benefits that OTS treatment gave in terms of passivating surface traps on SiO_2, this surface functionalisation does not completely eliminate surface SiOH groups,[43] and residual charge carrier traps remain at the semiconductor/dielectric interface.[43–45] Cytop is a fluoropolymer with a highly hydrophobic surface, leading to an extremely low trap density,[46] whilst simultaneously encapsulating the organic semiconductor film underneath.[39,47] Indeed, OFETs in this geometry exhibited similar electrical performance irrespective of measurement environment; representative transfer curves acquired in air and nitrogen are shown in Fig. S37. While the air stability of tetrathiocins has not been studied, it was previously observed that a co-polymer with a similarly sulfur-rich TTF unit exhibited excellent air stability.[48] Both the TTC compounds exhibited at least 10-fold higher hole mobilities when using Cytop dielectric compared to the devices on SiO_2 dielectric, along with lower threshold voltages and higher on/off ratios (see Tables 3 and 4).

To examine the effects of thermal treatment, we subjected these TGBC devices to similar annealing protocol to the SiO_2 devices (60 °C, 120 °C). We observed similar trends, see the summary of device properties in Tables 3 and 4 and representative transfer and output characteristics in Fig. S38 and S39. OFETs based on **5T-TTC** exhibited higher mobilities, however, the non-uniformity of the film resulted in greater mobility variations and lower number of working devices on the same substrate. In contrast, **EH-5T-TTC** based devices demonstrated slightly lower mobilities, but formed more uniform films, possibly due to the fact that the ethyl-hexyl branched units enabled better solution processibility. This led to a narrower mobility distribution and higher number of functional devices per substrate, in agreement with the AFM analysis (Fig. 8 and Fig. S36). Mobility histograms at different annealing temperatures are provided in Fig. S40. In Fig. S41 we plot the dependence of device mobility on the channel length for each device type. We observe negligible dependence of mobility on geometrical parameters, indicating that the contact resistance is sufficiently low to ensure the extracted mobility values accurately reflect the intrinsic properties of the **EH-5T-TTC** and **5T-TTC** organic semiconductors.

Summary

We have reported the synthesis of four organic semiconductors possessing a structural 'double-cable' motif with parallel conjugated chains held together through a fused tetrathiocin heterocycle. The conjugated chains consist of linear oligothiophenes, with either 3, 5 or 7 thiophenes in each chain. The single-crystal X-ray structures of three of the compounds featured in the work show that: (i) at least 5 thiophenes are required to provide a co-planar conformation within the conjugated units, and (ii) the tetrathiocin ring provides S···S short contacts between molecules, which in turn increases the bulk dimensionality of the organic semiconductor. Bottom-gate/bottom-contact and top-gate/bottom-contact OFET devices were prepared using a range of solvents for processing, different

annealing conditions and OTS and/or PFBT as SAMs. It was found that the septithiophene derivative **7T-TTC** gave hole mobilities greatly inferior to the quinquithiophene derivatives (2.8×10^{-5} cm^2 V^{-1} s^{-1} and with a low on/off ratio). Average hole mobilities for the devices containing compounds **5T-TTC** or **EH-5T-TTC** were consistently found to be in the range of 10^{-3} cm^2 V^{-1} s^{-1} to 10^{-2} cm^2 V^{-1} s^{-1}, and with good to high on/off ratios, with the highest μ_h value recorded for a device containing **5T-TTC** (7.3×10^{-2} cm^2 V^{-1} s^{-1}). The intrinsic charge transport properties of these double-cable tetrathiocin materials are supported by the two-dimensional nature of the semiconductor in the bulk, and it is shown here that the tetrathiocin core, which provides the double-cable structural motif, is superior to other such bridging heterocyclic species, *viz.* **5T-TTF** and **5T-Ge** (Fig. 1), which give hole mobilities of 8.6×10^{-3} cm^2 V^{-1} s^{-1} and 4.2×10^{-5} cm^2 V^{-1} s^{-1}, respectively. Double-cable tetrathiocin compounds therefore represent an exciting new material for organic field-effect transistors.

Conflicts of interest

There are no conflicts to declare.

Data availability

Data for this manuscript are available in two formats: (1) experimental procedures and routine characterisation for new compounds, thermal analyses plots, AFM images, and data in the form of graphs for OFET characterisation are provided in the SI as a separate file. See DOI: **https://doi.org/10.1039/d5tc02038g**.

(2) Supporting raw data for the manuscript can be accessed at the following address: **https://doi.org/10.5525/gla.researchdata.1940**.

CCDC 2453434–2453436 contain the supplementary crystallographic data for this paper.[49–51]

Acknowledgements

RGDT, JC and PJS thank the EPSRC for funding (EP/L012200/1 and EP/T022477/1). The work at Wake Forest University (M. M. and O. D. J.) was supported by the National Science Foundation under Awards ECCS-1810273 and DMR 2323423. LRS acknowledges support from the National Science Foundation Research Experience for Undergraduates Programme under award number CHE-0755206.

References

1 H. Sirringhaus, *Adv. Mater.*, 2005, **17**, 2411–2425.
2 G. Kim, S.-J. Kang, G. K. Dutta, Y.-K. Han, T. J. Shin, Y.-Y. Noh and C. Yang, *J. Am. Chem. Soc.*, 2014, **136**, 9477–9483.
3 A. F. Paterson, S. Singh, K. J. Fallon, T. Hodsden, Y. Han, B. C. Schroeder, H. Bronstein, M. Heeney, I. McCulloch and T. D. Anthopoulos, *Adv. Mater.*, 2018, **30**, 1801079.
4 Z. A. Lamport, K. J. Barth, H. Lee, E. Gann, S. Engmann, H. Chen, M. Guthold, I. McCulloch, J. E. Anthony, L. J. Richter, D. M. DeLongchamp and O. D. Jurchescu, *Nat. Commun.*, 2018, **9**, 5130.
5 M. Waldrip, Y. Yu, D. Dremann, T. Losi, B. Willner, M. Caironi, I. McCulloch and O. D. Jurchescu, *Adv. Mater.*, 2024, **36**, 2410442.
6 H. Dong, X. Fu, J. Liu, Z. Wang and W. Hu, *Adv. Mater.*, 2013, **25**, 6158–6183.
7 A. Wadsworth, D. Baran, J. Gorman and I. McCulloch, *Nanostructured Materials for Type III Photovoltaics*, The Royal Society of Chemistry, 2018, pp. 69–108, DOI: **10.1039/9781782626749-00069**.
8 J. Cameron, L. Nanson, N. Blouin, N. J. Findlay, A. R. Inigo and P. J. Skabara, *Org. Electron.*, 2017, **49**, 400–405.
9 A. C. Yeats, R. G. D. Taylor and P. J. Skabara, *Nanostructured Materials for Type III Photovoltaics*, The Royal Society of Chemistry, 2018, pp. 109–153, DOI: **10.1039/9781782626749-00109**.
10 F. Maleki, K. J. Thorley, H. F. Iqbal, D. Vong, T. Maitra, A. Petty, L. L. Daemen, S. R. Parkin, O. D. Jurchescu, J. E. Anthony and A. J. Moulé, *Chem. Mater.*, 2024, **36**, 4794–4805.
11 P. J. Skabara, J. B. Arlin and Y. H. Geerts, *Adv. Mater.*, 2013, **25**, 1948–1954.
12 J. Cameron, A. L. Kanibolotsky and P. J. Skabara, *Adv. Mater.*, 2024, **36**, 2302259.
13 H. Pang, F. Vilela, P. J. Skabara, J. J. W. McDouall, D. J. Crouch, T. D. Anthopoulos, D. D. C. Bradley, D. M. De Leeuw, P. N. Horton and M. B. Hursthouse, *Adv. Mater.*, 2007, **19**, 4438–4442.
14 M. Makala, Z. Xu, S. Saiev, X. Ni, S. Sabury, V. Coropceanu, J.-L. Brédas, Y. Diao, J. R. Reynolds, O. D. Jurchescu and A. M. Österholm, *Chem. Mater.*, 2025, **37**, 4145–4157.
15 I. A. Wright, N. J. Findlay, S. Arumugam, A. R. Inigo, A. L. Kanibolotsky, P. Zassowski, W. Domagala and P. J. Skabara, *J. Mater. Chem. C*, 2014, **2**, 2674–2683.
16 I. A. Wright, P. J. Skabara, J. C. Forgie, A. L. Kanibolotsky, B. González, S. J. Coles, S. Gambino and I. D. W. Samuel, *J. Mater. Chem.*, 2011, **21**, 1462–1469.
17 R. G. Taylor, J. Cameron, I. A. Wright, N. Thomson, O. Avramchenko, A. L. Kanibolotsky, A. R. Inigo, T. Tuttle and P. J. Skabara, *Beilstein J. Org. Chem.*, 2015, **11**, 1148–1154.
18 I. A. Wright, A. L. Kanibolotsky, J. Cameron, T. Tuttle, P. J. Skabara, S. J. Coles, C. T. Howells, S. A. J. Thomson, S. Gambino and I. D. W. Samuel, *Angew. Chem., Int. Ed.*, 2012, **51**, 4562–4567.
19 S. Arumugam, I. A. Wright, A. R. Inigo, S. Gambino, C. T. Howells, A. L. Kanibolotsky, P. J. Skabara and I. D. W. Samuel, *J. Mater. Chem. C*, 2014, **2**, 34–39.
20 L. K. Jagadamma, R. G. D. Taylor, A. L. Kanibolotsky, M. T. Sajjad, I. A. Wright, P. N. Horton, S. J. Coles,

I. D. W. Samuel and P. J. Skabara, *Sustainable Energy Fuels*, 2019, **3**, 2087–2099.
21 T. Shimizu and N. Kamigata, *J. Organomet. Chem.*, 2000, **611**, 106–115.
22 T. Shimizu, H. Murakami, Y. Kobayashi, K. Iwata and N. Kamigata, *Phosphorus, Sulfur Silicon Relat. Elem.*, 1999, **153**, 431–432.
23 T. Chivers, M. Parvez, I. Vargas-Baca and G. Schatte, *Can. J. Chem.*, 1998, **76**, 1093–1101.
24 D. J. Harrison and U. Fekl, *Chem. Commun.*, 2009, 7572–7574.
25 J. D. Wrixon, J. J. Hayward, O. Raza and J. M. Rawson, *Dalton Trans.*, 2014, **43**, 2134–2139.
26 J. D. Wrixon, Z. S. Ahmed, M. U. Anwar, Y. Beldjoudi, N. Hamidouche, J. J. Hayward and J. M. Rawson, *Polyhedron*, 2016, **108**, 115–121.
27 J. D. Wrixon, J. J. Hayward and J. M. Rawson, *Inorg. Chem.*, 2015, **54**, 9384–9386.
28 C. R. M. Asquith, M. L. Meli, L. S. Konstantinova, T. Laitinen, A. Poso, O. A. Rakitin, R. Hofmann-Lehmann, K. Allenspach and S. T. Hilton, *Bioorg. Med. Chem. Lett.*, 2015, **25**, 1352–1355.
29 T. Nakazawa, J. Xu, T. Nishikawa, T. Oda, A. Fujita, K. Ukai, R. E. P. Mangindaan, H. Rotinsulu, H. Kobayashi and M. Namikoshi, *J. Nat. Prod.*, 2007, **70**, 439–442.
30 P. A. Searle and T. F. Molinski, *J. Org. Chem.*, 1994, **59**, 6600–6605.
31 P. J. Skabara, I. M. Serebryakov, D. M. Roberts, I. F. Perepichka, S. J. Coles and M. B. Hursthouse, *J. Org. Chem.*, 1999, **64**, 6418–6424.
32 S. Zhang, M. A. Uddin, W. Zhao, L. Ye, H. Y. Woo, D. Liu, B. Yang, H. Yao, Y. Cui and J. Hou, *Polym. Chem.*, 2015, **6**, 2752–2760.
33 J. Rissler, *Chem. Phys. Lett.*, 2004, **395**, 92–96.
34 Z. A. Lamport, H. F. Haneef, S. Anand, M. Waldrip and O. D. Jurchescu, *J. Appl. Phys.*, 2018, 124.
35 N. Shirahata, W.-S. Seo, T. Kinoshita, T. Yonezawa, A. Hozumi, Y. Yokogawa, T. Kameyama, Y. Masuda and K. Koumoto, *Langmuir*, 2004, **20**, 8942–8946.
36 C. Goldmann, D. J. Gundlach and B. Batlogg, *Appl. Phys. Lett.*, 2006, 88.
37 O. D. Jurchescu, S. Subramanian, R. J. Kline, S. D. Hudson, J. E. Anthony, T. N. Jackson and D. J. Gundlach, *Chem. Mater.*, 2008, **20**, 6733–6737.
38 Y. Mei, D. Fogel, J. Chen, J. W. Ward, M. M. Payne, J. E. Anthony and O. D. Jurchescu, *Org. Electron.*, 2017, **50**, 100–105.
39 M. Makala, M. Barłóg, D. Dremann, S. Attar, E. G. Fernández, M. Al-Hashimi and O. D. Jurchescu, *J. Mater. Chem. C*, 2024, **12**, 17089–17098.
40 M. Waldrip, O. D. Jurchescu, D. J. Gundlach and E. G. Bittle, *Adv. Funct. Mater.*, 2020, **30**, 1904576.
41 J. W. Ward, M. A. Loth, R. J. Kline, M. Coll, C. Ocal, J. E. Anthony and O. D. Jurchescu, *J. Mater. Chem.*, 2012, **22**, 19047–19053.
42 S. Nagamatsu, K. Kaneto, R. Azumi, M. Matsumoto, Y. Yoshida and K. Yase, *J. Phys. Chem. B*, 2005, **109**, 9374–9378.
43 D. L. Angst and G. W. Simmons, *Langmuir*, 1991, **7**, 2236–2242.
44 H. F. Haneef, A. M. Zeidell and O. D. Jurchescu, *J. Mater. Chem. C*, 2020, **8**, 759–787.
45 H. F. Iqbal, M. Waldrip, H. Chen, I. McCulloch and O. D. Jurchescu, *Adv. Electron. Mater.*, 2021, **7**, 2100393.
46 P. J. Diemer, Z. A. Lamport, Y. Mei, J. W. Ward, K. P. Goetz, W. Li, M. M. Payne, M. Guthold, J. E. Anthony and O. D. Jurchescu, *Appl. Phys. Lett.*, 2015, 107.
47 H. F. Iqbal, Q. Ai, K. J. Thorley, H. Chen, I. McCulloch, C. Risko, J. E. Anthony and O. D. Jurchescu, *Nat. Commun.*, 2021, **12**, 2352.
48 D. Cortizo-Lacalle, S. Arumugam, S. E. T. Elmasly, A. L. Kanibolotsky, N. J. Findlay, A. R. Inigo and P. J. Skabara, *J. Mater. Chem.*, 2012, **22**, 11310–11315.
49 R. G. D. Taylor, J. Cameron, M. Fairley, I. A. Wright, L. R. Savagian, C. Wilson, M. B. Pitak, S. J. Coles, M. Makala, O. D. Jurchescu and P. J. Skabara, 2453434: Experimental Crystal Structure Determination, 2025, DOI: **10.5517/ccdc.csd.cc2nc013**.
50 R. G. D. Taylor, J. Cameron, M. Fairley, I. A. Wright, L. R. Savagian, C. Wilson, M. B. Pitak, S. J. Coles, M. Makala, O. D. Jurchescu and P. J. Skabara, 2453435: Experimental Crystal Structure Determination, 2025, DOI: **10.5517/ccdc.csd.cc2nc024**.
51 R. G. D. Taylor, J. Cameron, M. Fairley, I. A. Wright, L. R. Savagian, C. Wilson, M. B. Pitak, S. J. Coles, M. Makala, O. D. Jurchescu and P. J. Skabara, 2453436: Experimental Crystal Structure Determination, 2025, DOI: **10.5517/ccdc.csd.cc2nc035**.